Electromagnetic Behavior Simulation of REBCO Pancake Coils Considering REBCO Tape Rotation Under High Magnetic Field

So Noguchi, Takanobu Mato, Kwangmin Kim, and Seungyong Hahn

***Abstract*—Since the screening current induced in rare earth-barium-copper-oxide (REBCO) magnet generates an irregular magnetic field, a few screening current simulation methods have been proposed. For an insert REBCO magnet generating ultra-high magnetic field, a new screening current method has been proposed with consideration of the coil-deformation effect.**

In this paper, we have developed a new screening current method based on a partial element equivalent circuit (PEEC) model coupling with a two-dimensional stress finite element analysis to accurately the time-transient distribution of accurate screening current. In the presented method, the changes of self/mutual inductances are considered due to the coil deformation. As the simulation results, it was found that the coil deformation affected the screening current distribution. When considering the coil deformations, the screening current-induced fields to operating current are different for charging cycles. It is necessary to simulate the coil deformation to accurately estimate the screening current and the screening current-induced field.

***Index Terms*—Coil deformation, equivalent circuit model, REBCO magnet, numerical simulation, screening current.**

I. Introduction

SCREENING currents induced in high-temperature superconducting (HTS) coils are well-known as an embarrassing problem. For applications of magnetic resonance imaging (MRI) [1]–[3], nuclear magnetic resonance (NMR) [4]–[7], and particle accelerators [8]–[11], the screening current-induced field (SCIF) is undesirable. Hence, to reduce the SCIF, a few techniques such as a shaking field effect and an over-shooting method were proposed [12], [13].

Meanwhile, another problem on screening currents has arisen. It was pointed out that the screening currents cause excessive hoop stress [14], [15]. Some waviness or critical current degradation of rare-earth barium copper oxide (REBCO) tapes were actually observed in experiments after high magnetic field generation [6], [16]. Furthermore, Kolb-Bond *et al*. have suggested the REBCO tape rotation effect of REBCO pancake coils through the screening current simulation coupled with the elastic simulation [17]–[21]. In particular, an insert REBCO magnet in a high magnetic field generated by an outsert magnet is likely to deform because of high hoop stress. The screening currents generate unbalanced stresses, so that the REBCO tapes of the winding rotate. However, in the stress simulation, the insert REBCO coil was considered as a rigid body.

We have previously proposed a screening current simulation method based on a partial element equivalent circuit (PEEC) model [22]. In this paper, a two-dimensional (2D) stress finite element analysis (FEA) is coupled with the previously developed PEEC model. In 2D FEA, every turn is separately considered; i.e., two adjacent turns can stick or separate. As an object-contact problem, the Karush-Kuhn-Tucker condition is taken into account [23]. Using a newly developed method, the screening current distribution and the screening current-induced field (SCIF) are investigated. Depending on the deformed coil-shape, the different screening current is induced, and the SCIF does not follow the same hysteresis loop.

II. Deformation/Screening Current Simulation

To investigate the screening current-induced fields (SCIF) of REBCO pancake coils, we have developed the screening current simulation considering the REBCO tape rotation. In the developed method, the screening current and the elastic simulation are alternatively conducted as show in Fig. 1.

A. 2D Elastic Simulation

The coil deformation is simulated with two-dimensional (2D) finite element method (FEM) on the *rz* plane. The governing equations are as follows:

$$\begin{aligned} \frac{\partial \sigma_r}{\partial r} + \frac{\partial \sigma_{rz}}{\partial z} + \frac{\sigma_r - \sigma_\theta}{r} + J_\theta B_z &= \rho \frac{\partial^2 u_r}{\partial t^2} \\ \frac{\partial \sigma_{rz}}{\partial r} + \frac{\partial \sigma_z}{\partial z} + \frac{\sigma_{rz}}{r} - J_z B_r &= \rho \frac{\partial^2 u_z}{\partial t^2} \end{aligned} \quad (1)$$

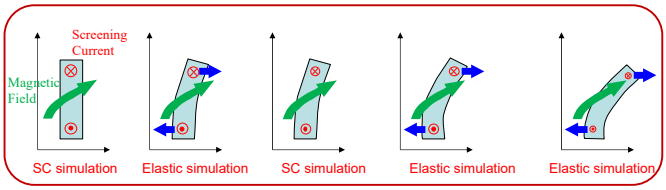

Fig. 1. Develop simulation method for screening current (SC) and elastic simulation. PEEC method and 2D FEM are used for SC and elastic simulation, respectively.

Manuscript received. This work was supported by the JSPS KAKENHI under Grant No. 20H02125. *(Corresponding author: So Noguchi.)*

S. Noguchi and T. Mato are with the Graduate School of Information Science and Technology, Hokkaido University, Sapporo 060-0814, Japan. (e-mail: noguchi@ssi.ist.hokudai.ac.jp).

K. Kim is the Magnet Science & Technology, National High Magnetic Field Laboratory, Tallahassee, FL 32310, USA (kwangmin.kim@magnet.fsu.edu).

S. Hahn is with the Department of Electrical and Computer Engineering, Seoul National University, Seoul 08826, Korea (e-mail: hahnsy@snu.ac.kr).

$$\begin{aligned}\varepsilon_r &= \frac{1}{E_r}\sigma_r - \frac{\nu_{\theta r}}{E_\theta}\sigma_\theta - \frac{\nu_{zr}}{E_z}\sigma_z \\ \varepsilon_\theta &= -\frac{\nu_{r\theta}}{E_r}\sigma_r + \frac{1}{E_\theta}\sigma_\theta - \frac{\nu_{z\theta}}{E_z}\sigma_z \\ \varepsilon_z &= -\frac{\nu_{rz}}{E_r}\sigma_r - \frac{\nu_{\theta z}}{E_\theta}\sigma_\theta + \frac{1}{E_z}\sigma_z\end{aligned} \tag{2}$$

$$\begin{aligned}\varepsilon_r &= \frac{\partial u_r}{\partial r} \\ \varepsilon_\theta &= \frac{u_r}{r} \\ \varepsilon_z &= \frac{\partial u_z}{\partial z}\end{aligned} \tag{3}$$

where σ_r, σ_θ, σ_{rz}, ρ, u_r, and u_z the radial, the hoop, the share stresses, the mass density, and the displacement in the radial and axial directions, respectively. ε_r, ε_θ, ε_z, E_r, E_θ, E_z, and ν_{12} are the strains in the radial, circumferential, and axial directions, the Young's moduli in the r, θ, and z directions, and the Poisson's ratio defined by $\nu_{12} = -\varepsilon_2/\varepsilon_1$. J_θ, J_z, B_r, and B_z, which are computed with the PEEC method explained later, are the current densities in the radial and axial directions and the magnetic fields in the r and θ directions.

B. Screening Current Simulation

We have previously developed the screening current (SC) simulation method based on a circuit model as shown in Fig. 2 [22]. Originally the partial element equivalent circuit (PEEC) model was extended for NI REBCO pancake coil, but the deformation effect was not considered.

In this paper, the SC PEEC method is newly improved to consider the deformation effect. The new governing equations are given as (4)–(6), where I, L, and R are the current, the inductance, and the resistance, respectively. m and n are the division number of the respective tape longitudinal and transverse directions. o is the number of contact resistances, and p is the number of pancake coils whose inductance is considered as a whole. The suffix is defined in Fig. 2.

Commonly the inducive voltage is represented by $L\mathrm{d}I/\mathrm{d}t$, and it is based on unchanged inductance. However, considering the coil deformation, the inductive voltage is newly obtained from $L\mathrm{d}I/\mathrm{d}t + I\mathrm{d}L/\mathrm{d}t$, because the self-/mutual inductances are changed with the coil deformation. In particular, for ultra-high magnetic field generation, the mutual inductances between insert and outsert magnets are largely changed; furthermore, the current of outsert magnets are large to generate a high magnetic field. Accordingly, the mutual-inductive voltage $I_{\mathrm{om}}\mathrm{d}M/\mathrm{d}t$ increases, where I_{om} and M are the current of outsert magnet and the mutual inductance between insert and outsert magnets.

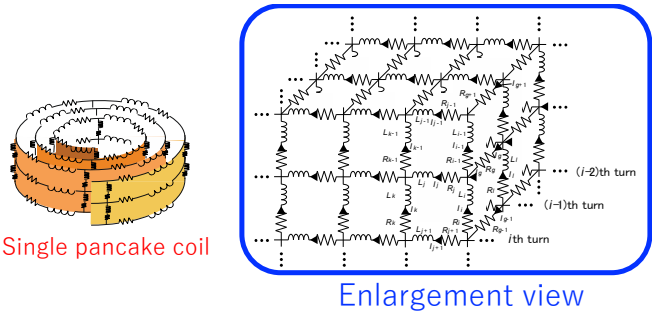

Fig. 2. Advanced partial element equivalent circuit (APEEC) model for computation of screening current of NI REBCO pancake coils.

Another modification of the coil deformation effect is the consideration of the angle of the magnetic field and the c-axis of deformed REBCO tape. In the developed method, the equivalent REBCO layer resistance R_{SC} is derived from the following relation based on the n-index power law:

$$R_{\mathrm{SC}} = \frac{\ell}{S}\frac{E_{\mathrm{c}}}{J}\left(\frac{J}{J_{\mathrm{c}}(B,\theta)}\right)^n \tag{8}$$

where ℓ, S, E_{c}, J, J_{c}, B, θ, and n are the length and area of REBCO tape, the electrical-field criteria (1 μV/cm in this paper), the current density, the critical current density, the magnetic field, its angle to the tape surface, and the power index, respectively. For non-deformed coil, the angle θ is the angle of the magnetic field from the radial direction; meanwhile, the angle θ is the angle of the magnetic field from the direction perpendicular to the wide REBCO tape surface which is tilted due to the coil deformation.

$$\begin{aligned}&\sum_m\left(L_{i,m}\frac{\mathrm{d}I_m}{\mathrm{d}t} + I_m\frac{\mathrm{d}L_{i,m}}{\mathrm{d}t}\right) + \sum_p\left(L_{i,p}\frac{\mathrm{d}I_p}{\mathrm{d}t} + I_p\frac{\mathrm{d}L_{i,p}}{\mathrm{d}t}\right) + R_iI_i + \sum_n\left(L_{j,n}\frac{\mathrm{d}I_n}{\mathrm{d}t} + I_n\frac{\mathrm{d}L_{j,n}}{\mathrm{d}t}\right) + \sum_p\left(L_{j,p}\frac{\mathrm{d}I_p}{\mathrm{d}t} + I_p\frac{\mathrm{d}L_{j,p}}{\mathrm{d}t}\right) + R_jI_j \\ &= \sum_m\left(L_{k,m}\frac{\mathrm{d}I_m}{\mathrm{d}t} + I_m\frac{\mathrm{d}L_{k,m}}{\mathrm{d}t}\right) + \sum_p\left(L_{k,p}\frac{\mathrm{d}I_p}{\mathrm{d}t} + I_p\frac{\mathrm{d}L_{k,p}}{\mathrm{d}t}\right) + R_kI_k + \sum_n\left(L_{j+1,n}\frac{\mathrm{d}I_n}{\mathrm{d}t} + I_n\frac{\mathrm{d}L_{j+1,n}}{\mathrm{d}t}\right) \\ &\quad + \sum_p\left(L_{j+1,p}\frac{\mathrm{d}I_p}{\mathrm{d}t} + I_p\frac{\mathrm{d}L_{j+1,p}}{\mathrm{d}t}\right) + R_{j+1}I_{j+1}\end{aligned} \tag{4}$$

$$\sum_m\left(L_{i,m}\frac{\mathrm{d}I_m}{\mathrm{d}t} + I_m\frac{\mathrm{d}L_{i,m}}{\mathrm{d}t}\right) + \sum_p\left(L_{i,p}\frac{\mathrm{d}I_p}{\mathrm{d}t} + I_p\frac{\mathrm{d}L_{i,p}}{\mathrm{d}t}\right) + R_iI_i + R_{g-1}I_{g-1} \tag{5}$$

$$\begin{aligned}&= \sum_m\left(L_{l,m}\frac{\mathrm{d}I_m}{\mathrm{d}t} + I_m\frac{\mathrm{d}L_{l,m}}{\mathrm{d}t}\right) + \sum_p\left(L_{l,p}\frac{\mathrm{d}I_p}{\mathrm{d}t} + I_p\frac{\mathrm{d}L_{l,p}}{\mathrm{d}t}\right) + R_lI_l + R_gI_g \\ &\cdots, h, \cdots, j-1, j, j+1, \cdots \in m \\ &\cdots, i-1, i, \cdots, k-1, k, \cdots, l, \cdots \in n \\ &\cdots, g-1, g, g+1, \cdots \in o \\ &\text{other pancake coils} \in p\end{aligned} \tag{6}$$

III. Simulation Results

To investigate the electromagnetic behaviors affected by the coil deformation, we employ, as a simulation model, an insert REBCO single pancake coil with 5 turns, which is placed inside a 31.1-T-generable outsert magnet. To increase the screening current, the insert REBCO coil is aligned off-center, upwards by 250 mm. Each turn is electrically insulated with Polymide tapes. The operating temperature is supposed to be 4.2 K.

As a charging/discharging pattern, the following steps are simulated:

(1) the outsert magnet charges up to 31.1 T at the magnet center,

(2) the insert REBCO coil charges to 400 A (1st charging), and then discharges to 0 A (1st discharging),

(3) the insert REBCO coil charges/discharges again (2nd charging/2nd discharging),

(4) the outsert magnet discharges down to 0 T,

(5) the outsert magnet charges up to 31.1 T again,

(6) the insert REBCO coil charges up to 400 A (3rd charging),

(7) the insert REBCO coil discharges (3rd discharging),

(8) the outsert magnet deenergize to 0 T at final.

Every ramping rate of the insert REBCO coil is 1 A/s. Fig. 4(a) shows the operating procedure.

A. Screening Current Distribution

Fig. 4(b) and (c) show the current density distribution maps with/without the consideration of the coil deformation, respectively.

1) Coil Deformation Consideration

As for the coil deformation case, at finishing charging the outsert magnet [① in Fig. 4(a)], the insert REBCO coil already deforms by the induced screening currents. Then, at ② after the 1st charging, the REBCO coil deforms the most. The amount of the deformation at ④ and ⑧ (2nd and 3rd charging) is smaller than that at ② (1st charging). Even at the same conditions (e.g., ③, ⑤, and ⑨ [the operating current I_{op} = 0 A, the background field B_{bg} = 31.1 T]), the screening current distributions and the deformed coil-shapes are slightly different. That is, the different deformed coil-shapes make the different screening current distribution, depending on the operation pattern.

2) No Coil Deformation Consideration

As for the no coil-deformation case, when the condition is the same (e.g., ③, ⑤, and ⑨ [I_{op} = 0 A, B_{bg} = 31.1 T]), the almost identical current distributions can be seen. Meanwhile, the current density distribution at ① is different from that at ⑦ in spite of the same condition. The charging history less affects the screening current due to no coil-deformation.

B. Screening Current-Induced Field

Next, the screening current-induced fields (SCIF) at the center of the insert coil are investigated, as shown in Fig. 3. Fig. 5 plots the SCIF with/without consideration of coil deformation, according to the operation pattern. Here, the

TABLE I
Specifications of Insert REBCO Single Pancake Coil and Condition

Number of pancake coils	1
Number of turns per single pancake	5
Inner diameter (mm)	120
REBCO tape width (mm)	4.0
REBCO tape thickness (mm)	0.1
Turn-to-turn insulation	Polymide tape
Operating temperature (K)	4.2

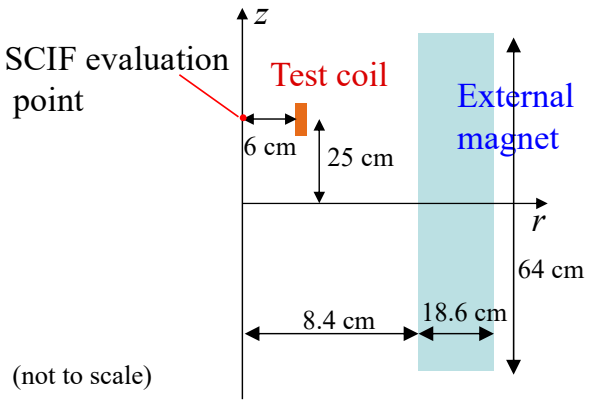

Fig. 3. Illustration of cross section of insert REBCO coil and outsert magnet.

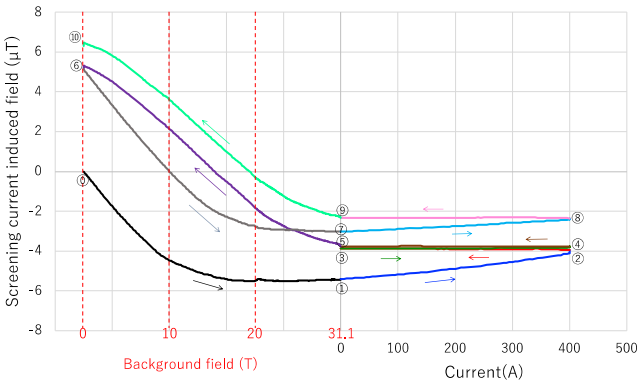

(a) with coil deformation

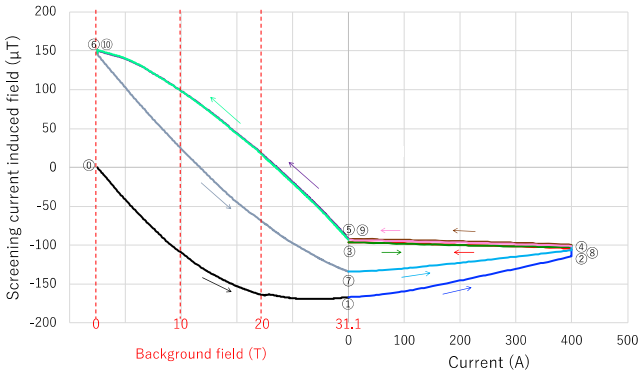

(b) without coil deformation

Fig. 5. Screening current-induced fields (a) with and (b) without consideration of coil deformation.

SCIF B_{sc} is defined as follows:

$$B_{SC} = B_{sim} - B_{hom} \quad (9)$$

where B_{sim} and B_{hom} are the simulated magnetic field and the magnetic field when the current is homogeneously distributes in the REBCO layer.

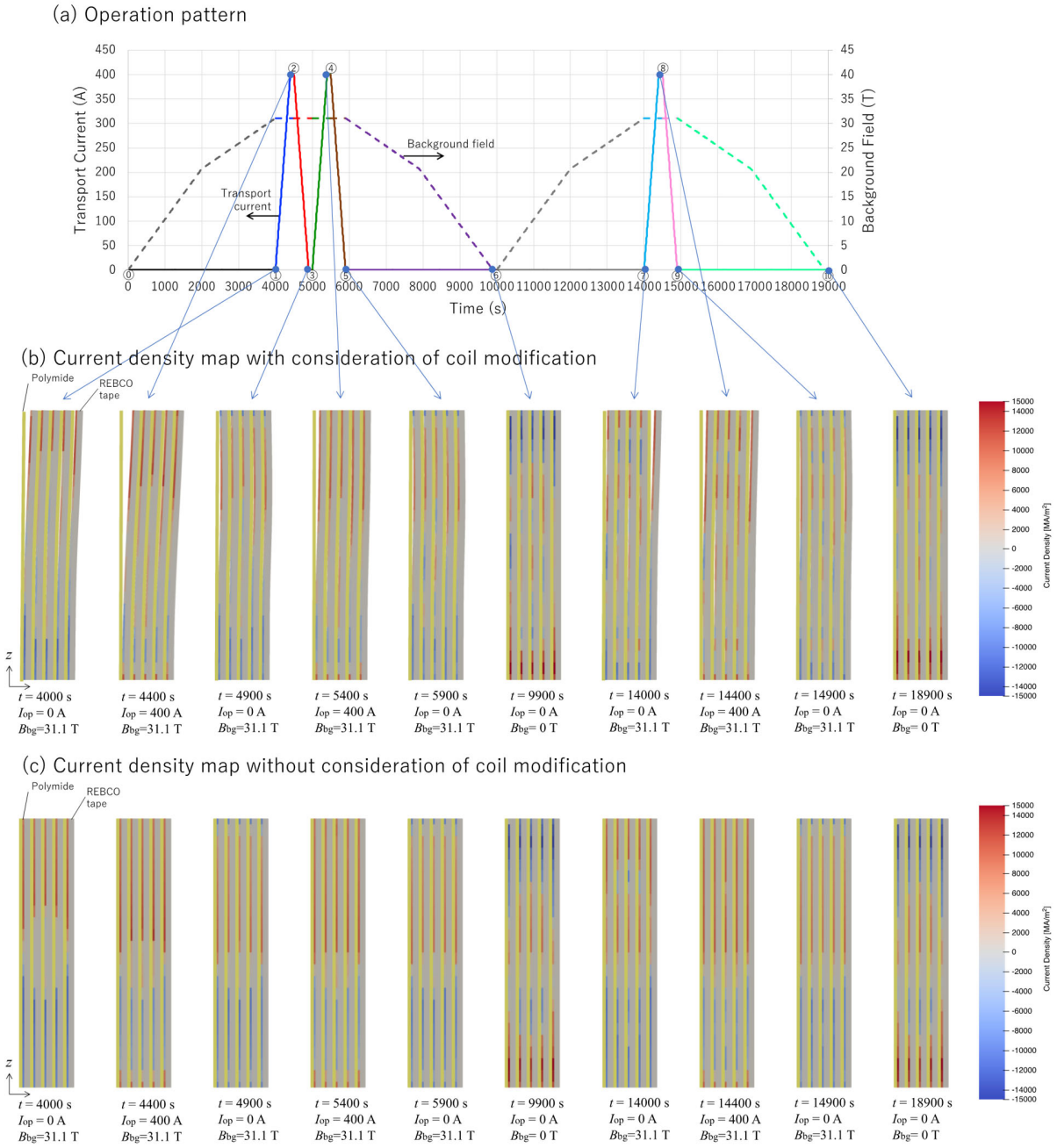

Fig. 4. Proposed ladder network equivalent circuit (LNEC) model. By stacking the PEEC model in the REBCO tape width direction, the LNEC model is constructed.

1) Coil Deformation Consideration

During the first external field generation, the SCIFs at I_{op} = 400 A are almost the same at ② and ④. However, at the second externa field generation, the SCIF at I_{op} = 400 A is completely different from that at the first time. Because, during charging/discharging the outsert magnet, the insert REBCO coil greatly deforms; i.e., the screening current distributions complicatedly differ even at the same conditions. Accordingly, the SCIF does not also follow the same hysteresis loop.

2) No Coil-Deformation Consideration

All the SCIFs at I_{op} = 400 A are very close each other. It means the screening current distributions are also very similar. The SCIF follows the same hysteresis loop except the first charging the insert and outsert magnets.

IV. Conclusion

In this paper, we have proposed a new screening current simulation method considering coil deformation. As a screening current simulation method, the partial element equivalent circuit (PEEC) model is extended to consider the change of self-/mutual inductances. As an elastic simulation method, the two-dimensional finite element analysis is employed. The hysteresis of the coil deformation affects the screening current distribution and the screening current-induced field.

REFERENCES

[1] T. Tosaka, *et al.*, "R&D project on HTS magnets for ultrahigh-field MRI systems," *IEEE Trans. Appl. Supercond.*, vol. 26, no. 4, Jun. 2016, Art. no. 4402505.

[2] H. Miyazaki, *et al.*, "Design of a conduction-cooled 9.4T REBCO magnet for whole-body MRI systems," *Supercond. Sci. Technol.*, vol. 29, no. 10, Oct. 2016, Art. no. 104001.

[3] S. Yokoyama, *et al.*, "Research and development of the high stable magnetic field ReBCO coil system fundamental technology for MRI," *IEEE Trans. Appl. Supercond.*, vol. 27, no. 4, Jun. 2017, Art. no. 4400604.

[4] Y. Iwasa, , *et al.*, "A high-resolution 1.3-GHz/54-mm LTS/HTS NMR magnet," *IEEE Trans. Appl. Supercond.*, vol. 25, no. 3, Jun. 2015, Art. no. 4300205.

[5] S. Noguchi, *et al.*, "Quench analyses of the MIT 1.3GHz LTS/HTS NMR magnet," *IEEE Trans. Appl. Supercond.*, vol. 29, no. 5, Aug. 2019, Art. no. 4301005.

[6] D. Park, *et al.*, "MIT 1.3-GHz LTS/HTS NMR magnet: post quench analysis and new 800-MHz insert design," *IEEE Trans. Appl. Supercond.*, vol. 29, no. 5, Aug. 2019, Art. no. 4300804.

[7] S. Iguchi, *et al.*, "Advanced field shimming technology to reduce the influence of a screening current in a REBCO coil for a high-resolution NMR magnet," *Supercond. Sci. Technol.*, vol. 29, no. 4, Apr. 2016, Art. no. 045013.

[8] H. Ueda, *et al.*, "Conceptual design of next generation HTS cyclotron," *IEEE Trans. Appl. Supercond.*, vol. 23, no. 3, Jun. 2013, Art. no. 4100205.

[9] J. Nugteren, G. Kirby, J. Murtomäki, G. DeRijk, L. Rossi, and A. Stenvall, "Toward REBCO 20 T+ dipoles for accelerators," *IEEE Trans. Appl. Supercond.*, vol. 28, no. 4, Jun. 2018, Art. no. 4008509.

[10] S. Takayama, *et al.*, "Development of an HTS accelerator magnet with REBCO coils for tests at HIMAC beam line," *IEEE Trans. Appl. Supercond.*, vol. 29, no. 5, Aug. 2019, Art. no. 4004205.

[11] H. Ueda, *et al.*, "Conceptual design of compact HTS cyclotron for RI production," *IEEE Trans. Appl. Supercond.*, vol. 29, no. 5, Aug. 2019, Art. no. 4101105.

[12] K. Kajikawa and Y. Okabe, "Reduction of screening-current-induced fields in an HTS tape winding using toroidal arrangement of shaking coil," *IEEE Trans. Appl. Supercond.*, vol. 26, no. 4, Jun. 2016, Art. no. 4400504.

[13] H. Miyazaki, *et al.*, "Screening-current-induced magnetic field of conduction-cooled HTS magnets wound with REBCO-coated conductors," *IEEE Trans. Appl. Supercond.*, vol. 27, no. 4, Jun. 2017, Art. no. 4701705.

[14] S. Hahn, K. L. Kim, K. Kim, K. Bhattarai, K. Radcliff, X. Hu, T. Painter, I. Dixon, and D. Larbalestier, "Progress in No-Insulation HTS Magnet Researches," *presented at Applied Superconductivity Conference 2018*.

[15] X. Hu, *et al.*, "Analyses of the plastic deformation of coated conductors deconstructed from ultra-high field test coils," *Supercond. Sci. Technol.*, vol. 33, no. 9, Sep. 2020, Art. no. 095012.

[16] S. Hahn, *et al*., "45.5-tesla direct-current magnetic field generated with a high-temperature superconducting magnet," Nature, vol. 570, pp. 496-499, Jun. 2019.

[17] D. Kolb-Bond, M. Bird, I. R. Dixon, and T. Painter, "Screening current rotation effects: SCIF and strain in REBCO magnets," *Supercond. Sci. Technol*., vol. 34, no. 9, Sep. 2021, Art. no. 095004.

[18] Y. Li, *et al*., "Screening-current-induced strain gradient on REBCO conductor: an experimental and analytical study with small coils wound with monofilament and striated multifilament REBCO tapes," *IEEE Trans. Appl. Supercond*., vol. 30, no. 4, 2020, Art no. 4702305.

[19] Y. Yan, *et al.*, "Screening-current-induced mechanical strains in REBCO insert coils," *Supercond. Sci. Tech*., vol. 35, no. 1, 2021, Art. no. 014003.

[20] Y. Yan, *et al.*, "Screening current induced magnetic field and stress in ultra-high-field magnets using REBCO coated conductors," *Supercond. Sci. Tech*., vol. 34, no. 8, 2021, Art. no. 085012.

[21] H. Ueda, *et al.*, "Experiment and numerical simulation of the combined effect of winding, cool-down, and screening current induced stresses in REBCO coils," *Supercond. Sci. Tech*., vol. 35, no. 5, 2022, Art. no. 054001.

[22] S. Noguchi and S. Hahn, "A newly developed screening current simulation method for REBCO pancake coils based on extension of PEEC model," *Supercond. Sci. Technol.*, vol. 35, no. 4, Mar. 2022, Art. no. 044005.

[23] H. W. Kuhn and A. W. Tucker, "Nonlinear programing," *Proceeding of the Second Berkeley Symposium on Mathematical Statics and Probability*, *University of California Press*, pp. 481–492, 1951.